

Spatial separation of large dynamical blueshift and harmonic generation

Mette B. Gaarde* and Mitsuko Murakami

Department of Physics and Astronomy, Louisiana State University, Baton Rouge, Louisiana 70803-4001, USA

Reinhard Kienberger

Max Planck Institute for Quantum Optics, Garching, D-85748 Germany

(Received 26 April 2006; published 2 November 2006)

We study the temporal and spatial dynamics of the large amplitude and frequency modulation that can be induced in an intense, few cycle laser pulse as it propagates through a rapidly ionizing gas. Our calculations include both single atom and macroscopic interactions between the nonlinear medium and the laser field. We analyze the harmonic generation by such pulses and show that it is spatially separated from the ionization dynamics which produce a large dynamical blueshift of the laser pulse. This means that small changes in the initial laser focusing conditions can lead to large differences in the laser frequency modulation, even though the generated harmonic spectrum remains essentially unchanged. We also show that the ionization dynamics strongly influences the possibility of synthesizing isolated attosecond pulses.

DOI: [10.1103/PhysRevA.74.053401](https://doi.org/10.1103/PhysRevA.74.053401)

PACS number(s): 32.80.Wr, 42.65.Re, 42.65.Jx, 42.65.Ky

I. INTRODUCTION

In their pioneering experiments reported in [1], Hentschel *et al.* demonstrated the generation of single attosecond XUV pulses by 7 fs, 750 nm laser pulses interacting with a neon gas. As a first application, these XUV pulses were used to probe the subcycle time dependence of the laser electric field emerging from the neon gas. A surprisingly large dynamical blueshift was observed in this way, with a maximum value of approximately 35% of the laser frequency, a result which was not well reproduced by theory.

Ionization is intrinsic to all highly nonlinear laser matter interactions. It contributes free electrons to the interaction medium which induces a temporal and spatial variation in the refractive index during propagation. This causes both self-phase modulation and defocusing of the field [2]. The experimental results in [1] raise a number of questions: (i) Can such a large frequency modulation be caused by ionization driven self-phase modulation? (ii) If so, how is it consistent with the observed harmonic cutoff energy around 90 eV, which indicates a relatively moderate interaction intensity around 5×10^{14} W/cm² [3]? And (iii) what are the consequences of the ionization dynamics for the spectral and temporal properties of the generated XUV radiation, in particular the XUV radiation around the cutoff energy which is used to synthesize attosecond pulses?

In this paper, we answer these questions by analyzing the temporal and spatial ionization dynamics of an intense few-cycle pulse as it propagates through a neon gas cell and generates harmonics [4], using parameters similar to those of the experiment in [1]. We show that in the beginning of the gas cell a large laser frequency modulation builds up rapidly when the intensity is still high, and then slows down toward the end of the cell because the intensity is reduced by defocusing. We find that, quite generally, the harmonic generation is spatially separated from the frequency modulation of the

driving field since the XUV radiation is built up predominantly in the second half of the medium. Furthermore, we show that the frequency modulation is very sensitive to small changes in the initial focusing conditions of the laser beam, whereas the intensity of the beam after propagation and the harmonic spectrum is not. Therefore, even though the XUV pulse is an ideal probe of the laser field after its interaction with the gas, the harmonic spectrum and in particular its cutoff energy are poor indicators of the magnitude of the ionization driven dynamics. Finally, we show that also the formation of single attosecond XUV pulses is very sensitive to the propagation dynamics of the fundamental, and that the most favorable generating conditions are those in which the ionization dynamics give rise to a large frequency modulation and spatiotemporal reshaping of the laser pulse.

II. THEORETICAL METHOD

Our description of the intense-laser matter interaction includes both the response of a single atom to the laser pulse and the collective response of the macroscopic gas to the focused laser beam via the coupled, nonadiabatic solutions to the Maxwell wave equation and the time-dependent Schrödinger equation (TDSE).

We solve the wave equation for the driving and the generated fields in the slowly evolving wave approximation which is valid for driving pulses as short as one optical cycle [4]. We follow an approach similar to that outlined in [5], in which the wave equation has the following form, in a coordinate system that moves with the driving pulse:

$$\nabla_{\perp}^2 \tilde{E}_1(\omega) + \frac{2i\omega}{c} \frac{\partial \tilde{E}_1(\omega)}{\partial z} = \mu_0 \tilde{G}(\omega), \quad (1)$$

$$\begin{aligned} \nabla_{\perp}^2 \tilde{E}_h(\omega) + \frac{2i\omega}{c} \frac{\partial \tilde{E}_h(\omega)}{\partial z} = & + \mu_0 [\tilde{G}(\omega) - \omega^2 \tilde{P}_{nl}(\omega)] \\ & - \frac{i\omega}{c} \tilde{\alpha}(\omega) \tilde{E}_h(\omega), \end{aligned} \quad (2)$$

where all the frequency dependent quantities $\tilde{E}_1(\omega)$, $\tilde{G}(\omega)$,

*Electronic address: gaarde@phys.lsu.edu

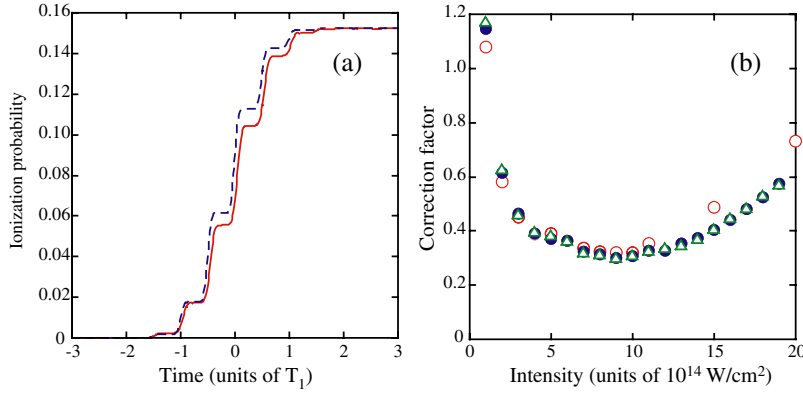


FIG. 1. (Color online) (a) Time dependent ionization probability of a neon atom exposed to a 750 nm, 7 fs laser pulse with a peak intensity of 10^{15} W/cm 2 . $P_{\text{vol}}(t)$ is shown with a solid line; $\beta P_{\text{ADK}}(t)$ is shown with a dashed line. $T_1 = 2.5$ fs is the optical period of the driving field. (b) Intensity dependent correction factor β for three different pulses: 7 fs duration, cosine carrier (open circles), 5 fs duration, cosine carrier (open triangles), and 5 fs duration, sine carrier (filled circles).

$\tilde{\alpha}(\omega)$, $\tilde{E}_h(\omega)$, and $\tilde{P}_{\text{nl}}(\omega)$ are also functions of the cylindrical coordinates r , z .

We solve Eqs. (1) and (2) for the driving field $\tilde{E}_1(\omega)$ and the generated fields $\tilde{E}_h(\omega)$ in the frequency domain, by space-marching through the ionizing nonlinear medium [6]. At each plane in the propagation direction z , we calculate the time-dependent driving field $E_1(t)$ as the Fourier transform of $\tilde{E}_1(\omega)$. We then calculate the nonlinear atomic response in the time domain by solving the TDSE using $E_1(t)$ as the driving field (see below). The time-dependent atomic response is used to calculate the frequency-dependent source terms in the wave equation, $\tilde{P}_{\text{nl}}(\omega)$ and $\tilde{G}(\omega)$, for marching to the next plane in z . Absorption of the generated radiation is included for all frequencies above the ionization threshold of neon via the absorption coefficients $\tilde{\alpha}(\omega)$ obtained from [7]. The absorption coefficient is proportional to the density of neutral atoms, $N_0 - N_e(t)$, where N_0 is the initial density and $N_e(t)$ is the time-dependent electron density (see below).

The source term for the generated radiation, $\tilde{P}_{\text{nl}}(\omega)$, is calculated from the time-dependent nonlinear polarization field, which is taken to be proportional to the microscopic single atom dipole moment $d_{\text{nl}}(t)$ and the density of neutral atoms:

$$\tilde{P}_{\text{nl}}(\omega) = \tilde{F}[(N_0 - N_e(t))d_{\text{nl}}(t)], \quad (3)$$

where \tilde{F} denotes a Fourier transform. Both the atomic density and the dipole moment also depend on r and z . $d_{\text{nl}}(t)$ is calculated by solving the TDSE, using a nonadiabatic form of the strong field approximation which takes into account the full time dependence of the driving field $E_1(t)$ [10].

The source term $\tilde{G}(\omega)$ for the propagation of the fundamental is due to the ionization of the medium, and is calculated from the time-dependent current density $J(t)$, $\tilde{G}(\omega) = \tilde{F}[\partial J(t)/\partial t]$. We follow the approach in [2] and include two contributions to the current density:

$$\frac{\partial J_p(t)}{\partial t} = \frac{e^2 N_e(t)}{m_e} E_1(t), \quad (4)$$

$$\frac{\partial J_{\text{abs}}(t)}{\partial t} = \frac{\partial}{\partial t} \frac{\gamma(t) N_e(t) I_p E_1(t)}{|E_1(t)|^2}, \quad (5)$$

where e and m_e are the electron charge and mass, $\gamma(t)$ is the ionization rate, and I_p is the atomic ionization potential. The plasma oscillation term $J_p(t)$ is due to the oscillatory motion of the free electrons in the laser electric field, and gives rise to a spatial and temporal variation of the refractive index which causes defocusing and self-phase modulation. The absorption term $J_{\text{abs}}(t)$ describes the loss of energy from the laser field due to the ionization of the medium. This term is small for all the cases discussed in this paper.

To describe the short pulse ionization dynamics correctly it is crucial to accurately calculate $N_e(t)$ and $\gamma(t)$ with sub-cycle precision. Our calculation of $N_e(t)$ originates in a numerical solution of the TDSE within the single active electron approximation [8]. We define the ionization probability $P_{\text{vol}}(t)$ from the probability density of the wave function outside of a small volume around the ion core, which can be continuously evaluated during the calculation. In Fig. 1(a) we show $P_{\text{vol}}(t)$ (solid line) for a 750 nm, 7 fs driving pulse with a peak intensity of 10^{15} W/cm 2 . Because of its short duration, the ionization probability at the end of the pulse is only about 15%.

Ideally, we would directly couple our numerical solution of the TDSE to the solution of the wave equation and use $P_{\text{vol}}(t)$ to describe the time dependent ionization. Currently, we do not have the computational apparatus to do so. We also cannot directly use the instantaneous tunnel ionization rates proposed by Ammosov, Delone, and Krainov (ADK) [9] since these give rise to much larger ionization probabilities at high intensities than the numerical TDSE solution. However, we find that for a given peak intensity, the ionization probability $P_{\text{ADK}}(t)$ calculated from ADK rates differs from $P_{\text{vol}}(t)$ by only a constant factor β , as long as the intensity is below the (ADK) saturation intensity. We determine β as the ratio between $P_{\text{vol}}(t)$ and $P_{\text{ADK}}(t)$ at the end of the laser pulse. The dashed line in Fig. 1(a) shows $\beta P_{\text{ADK}}(t)$ which is in excellent agreement with $P_{\text{vol}}(t)$.

We next calculate $\beta(I_0)$ by comparing $P_{\text{ADK}}(t)$ and $P_{\text{vol}}(t)$ for many different peak intensities I_0 . This function is shown in Fig. 1(b) as open circles. We have calculated $\beta(I_0)$ for different pulse durations and find that it depends only weakly on the duration and the absolute phase of the driving pulse.

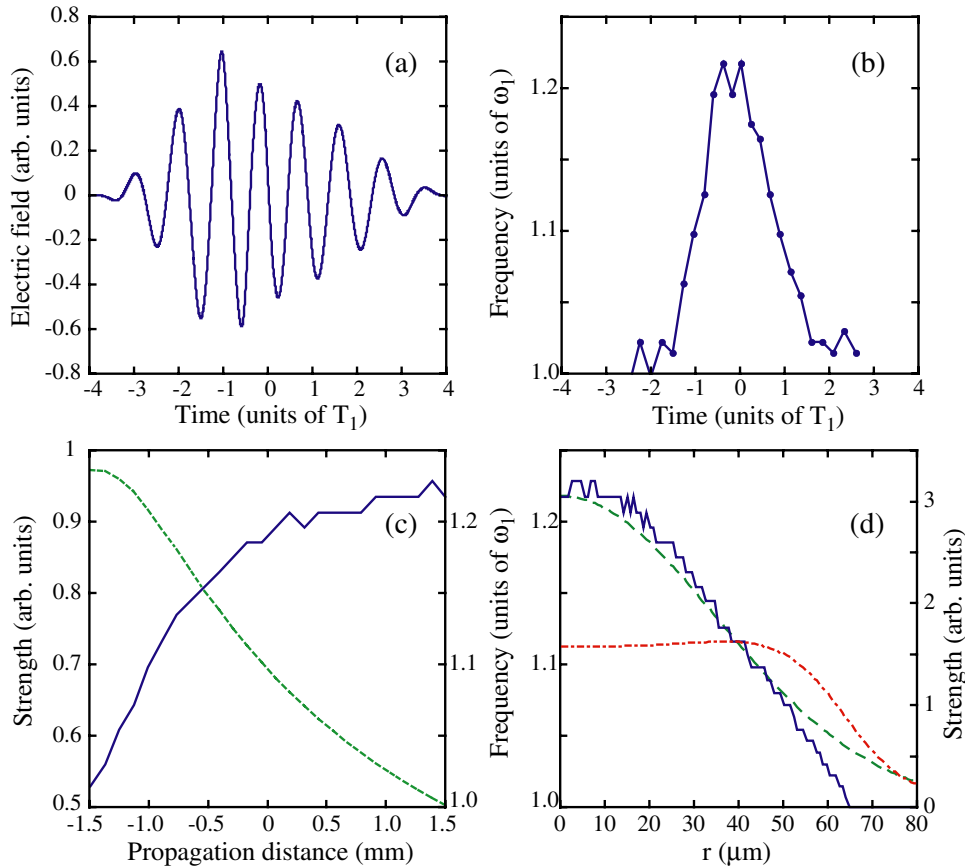


FIG. 2. (Color online) Spatiotemporal dynamics of frequency modulation of 750 nm, 7 fs pulse propagating through 3 mm of neon gas. The time-dependent amplitude and frequency of the laser electric field at the end of the neon gas is shown in (a) and (b), respectively. Figure (c) shows the maximum of the instantaneous frequency (solid line, right axis) and the on-axis energy density (dashed line, left axis) versus propagation distance. The radial variation of the maximum instantaneous frequency at the end of the gas is shown in (d) (solid line, left axis), along with the laser intensity at the beginning and at the end of the medium (dashed and dot-dashed, right axis).

Examples are shown in Fig. 1(b) for driving pulse durations of 5 fs and two different carrier envelope phases. Finally, we use $\beta(I_0)P_{\text{ADK}}(t)$ to calculate the source terms $N_e(t)$ and $\gamma(t)$ for each point in the nonlinear medium, where I_0 is the peak intensity of the driving pulse at that point. The insensitivity of $\beta(I_0)$ to the duration and phase of the driving pulse ensures that this is justified even as the pulse changes shape and phase during propagation.

III. RESULTS

Figure 2 illustrates the spatial and temporal dynamics of the frequency modulation experienced by a laser pulse during propagation through a rapidly ionizing neon gas. As in [1], the incoming laser pulse has a wavelength of 750 nm and a duration of 7 fs. The laser beam has a confocal parameter of 4.2 cm and its focus is in the center of a 3 mm long neon gas jet with a density of $5 \times 10^{18} \text{ cm}^{-3}$. In the absence of the nonlinear medium the peak intensity in the focus would be $9 \times 10^{14} \text{ W/cm}^2$.

In Fig. 2(a) we show the on-axis electric field of the laser pulse after propagation through the neon gas. Its time dependent frequency, shown in Fig. 2(b), is calculated from the separation between consecutive peaks and zeros of the electric field in Fig. 2(a). The pulse exhibits a large frequency chirp with a shape characteristic of self-phase modulation. The maximum blueshift which occurs near the peak of the pulse is very large, approximately 22%.

Figure 2(c) shows how this large blueshift is accumulated during propagation. The dashed line (left axis) shows the

on-axis energy density and the solid line (right axis) shows the blueshift, as functions of the propagation distance z . At each point in z , the blueshift has been found as the maximum value of the instantaneous frequency as plotted in Fig. 2(b). At the beginning of the gas where the intensity is high, defocusing is very strong. The energy density is reduced by almost a factor of 2 by the end of the gas. This intensity variation in turn controls the buildup of the blueshift which accumulates rapidly in the first half of the gas and saturates towards the end.

The solid line in Fig. 2(d) shows the radial variation of the blueshift at the end of the gas (left axis). The blueshift is largest on axis and decreases as a function of r . The dashed and dot-dashed lines (right axis) show the radial variation of the laser intensity at the beginning and at the end of the medium, respectively. The radial variation of the blueshift closely follows that of the incoming laser field, in agreement with the result in (c) that the blueshift is predominantly generated at the beginning of the gas. Experimentally, the laser field is probed by the XUV pulse after refocusing both beams in to a second gas jet by a mirror placed several meters from the first jet [1]. The focusing mirror is much smaller than the laser beam and therefore the XUV pulse only probes its on-axis frequency modulation [11]. In principle, the radial variation of the dynamical blueshift could be probed by slightly misaligning the two beams.

The ionization driven dynamics of the laser pulse has important consequences for the harmonic generation, and therefore for the formation of attosecond XUV pulses as these are synthesized from a range of harmonics near the cutoff [1].

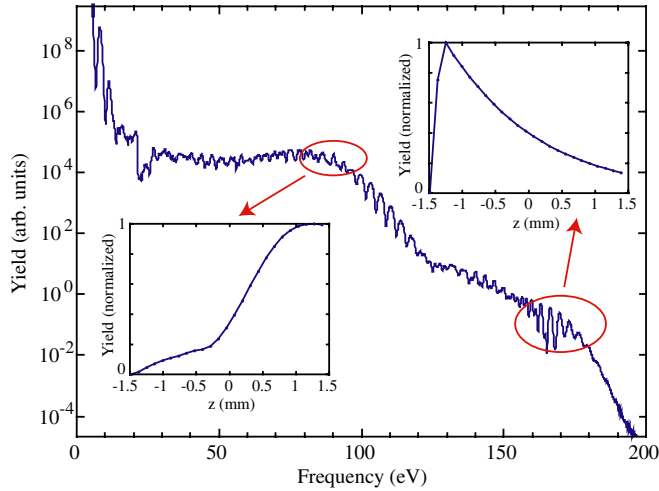


FIG. 3. (Color online) Radially integrated harmonic spectrum at the end of the neon gas. The insets show the buildup along the propagation direction of the XUV radiation around 90 and 155 eV (left and right inset, respectively).

Figure 3 shows the radially integrated harmonic spectrum at the end of the neon gas. As a result of the frequency shift of the laser pulse, the harmonic structures in the spectrum are not at odd multiples of the incoming laser frequency. As a result of the defocusing of the laser beam, the harmonic spectrum exhibits two different cutoffs. The high energy cutoff around 170 eV is determined by the peak intensity of the incoming beam ($\approx 9 \times 10^{14}$ W/cm²) [3], whereas the dominant low energy cutoff around 90 eV corresponds to the reduced peak intensity in the second half of the medium. In an experiment, it is likely that only the low energy cutoff would be observed as the high energy cutoff is orders of magnitude weaker [12]. For the remainder of this paper, we will therefore be referring only to the low energy cutoff when we discuss the cutoff energy of the harmonic spectrum.

The insets show how the XUV radiation around 90 eV (left inset) and above 155 eV (right inset) builds up during propagation. The highest energies are only generated over a short distance in the beginning of the medium and are then reabsorbed through the remainder of the gas. In contrast, the 90 eV photons are generated all through the medium. The saturation of this signal at the end of the medium is due to phase matching. For longer propagation lengths one would observe a periodic increase and decrease of the yield. The

total energy in a 5 eV range around 90 eV is approximately 10 pJ.

Figure 3 shows that the harmonic spectrum and its cutoff energy are poor indicators of the propagation dynamics of the driving field. In a rapidly ionizing, long medium the harmonic generation is spatially separated from the defocusing and self-phase modulation experienced by the laser field. In particular, both the yield and the photon energy of the spectral cutoff are essentially decoupled from the dynamical blueshift of the laser pulse.

This decoupling is further demonstrated in Fig. 4. We show results of a calculation where the focusing conditions of the incoming laser beam have been slightly changed compared to Fig. 2 while its energy has been kept constant. The new beam has a tighter focus with a confocal parameter of 3 cm and a peak intensity of 12.6×10^{14} W/cm². This corresponds to decreasing the beam waist by less than 20%.

Figure 4(a) compares the propagation dynamics of the two laser beams, showing the z dependence of the on-axis energy density and the on-axis maximum frequency shift, as in Fig. 2(c). The higher initial intensity gives rise to more free electrons, which in turn cause stronger defocusing. This means that the two beams have almost identical intensities at the end of the medium, and therefore give rise to very similar harmonic spectra, as shown in Fig. 4(b). However, the peak dynamical blueshift of the more tightly focused beam is much higher than before and reaches almost 35% by the end of the medium. We have also calculated the frequency modulation and the harmonic spectrum of a more loosely focused laser beam than those shown in the figure. A laser pulse with an initial peak intensity of 5×10^{14} W/cm² and a confocal parameter of 6 cm experiences only a marginal spatiotemporal reshaping due to ionization, leading to an intensity reduction of about 10% and a blueshift of less than 5% (not shown in Fig. 4). This pulse also generates a harmonic spectrum with a 90 eV cutoff and a shape very similar to the ones shown in the figure.

The discussion above answers the first two questions posed in the Introduction: (i) Ionization induced self-phase modulation can indeed induce a very large laser frequency shift in conditions very similar to those in [1] and (ii) because the laser pulse dynamics is spatially separated from the harmonic generation, the harmonic cutoff energy is essentially decoupled from the magnitude of the blueshift.

Figure 5 addresses the third question in the Introduction about the influence of the ionization dynamics on the tempo-

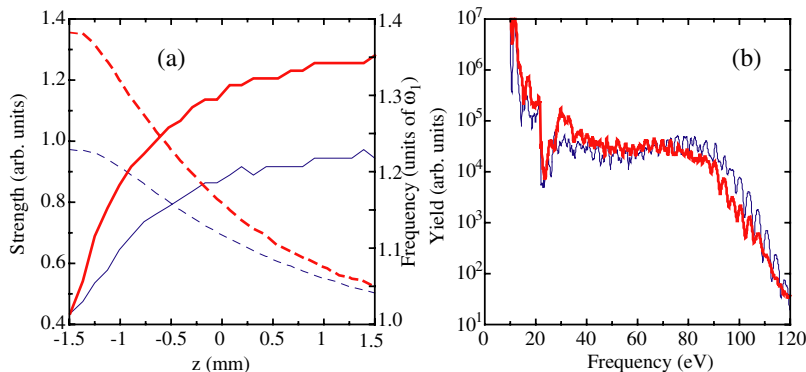


FIG. 4. (Color online) We compare the buildup of the frequency modulation and the harmonic spectrum generated by two laser beams with the same energy but slightly different focusing conditions. Thick lines show results of a more tightly focused beam than that used in Figs. 2 and 3 (thin lines).

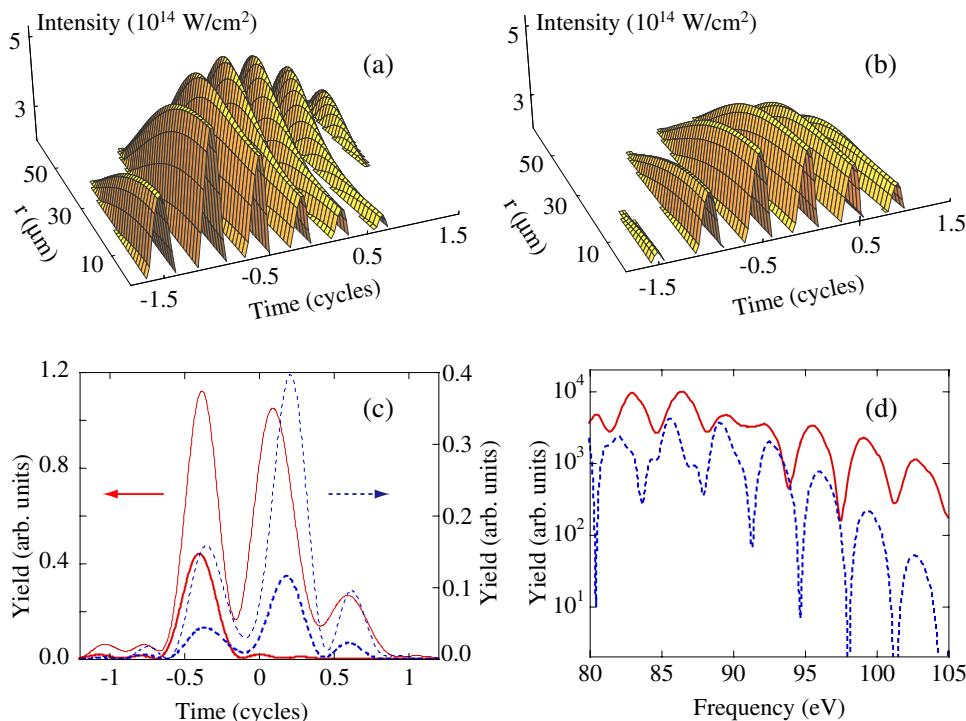


FIG. 5. (Color online) (a) and (b) Spatiotemporal profiles of the laser pulse at the end of the neon gas. In (a) we have used conditions as in Fig. 3, and (b) shows a laser pulse that gives rise to the same harmonic cutoff energy around 90 eV, but has a lower initial peak intensity ($5 \times 10^{14} \text{ W/cm}^2$). In (c) we show time profiles of a 5 eV range around 90 eV generated by the laser pulses in (a) and (b) (solid and dashed lines, respectively). Thin lines indicate the time profiles in the near field at the end of the neon gas and thick lines the time profile after reflection and refocusing by a small mirror placed in the far field. The spectra corresponding to the refocused XUV time profiles are shown in (d).

ral and spectral structure of the high energy XUV radiation which is used to synthesize attosecond pulses. Figures 5(a) and 5(b) show the three-dimensional spatiotemporal profile of the intensity of two different laser pulses at the end of the neon gas. In Fig. 5(a) we have used laser parameters as in Fig. 2, and in Fig. 5(b) the laser intensity is lower ($5 \times 10^{14} \text{ W/cm}^2$) and the confocal parameter is longer (6 cm). The propagation dynamics for these two pulses are very different. In Fig. 5(a), the strong temporal and spatial reshaping of the laser beam that takes place in the beginning of the medium results in a broad, divergent beam, in which the peak of the pulse occurs at different times for different radial positions. In Fig. 5(b), the lower peak intensity means that the pulse propagates through the medium essentially unaltered. The two different pulses both give rise to a harmonic cutoff energy around 90 eV and very similar harmonic spectra as discussed in connection with Fig. 4.

The XUV radiation near the cutoff energy is only generated at the highest intensities [13]. The laser pulse shown in Fig. 5(a) will give rise to one XUV burst on axis, and one or several bursts off axis half a cycle later [14]. The radially integrated time profile at the end of the nonlinear medium therefore contains several attosecond bursts, as shown in Fig. 5(c) for a 5 eV range of radiation around 90 eV (thin solid line). However, since the off-axis XUV radiation is generated by a strongly divergent wave front and is much less collimated than the on-axis XUV radiation, spatial filtering in the far field leads to the selection of a single attosecond burst generated on or close to the axis [14] (thick solid line). The spatial filter is a mirror with a diameter of 2 mm, placed 3 m from the neon source, which reflects and refocuses the XUV radiation as was done in [1]. In contrast, spatial filtering does not alter the time structure of the XUV radiation generated by the laser pulse in Fig. 5(b). This is demonstrated by the

near field and refocused time profiles shown in Fig. 5(c) (thin and thick dashed lines, respectively) which both contain multiple attosecond bursts. This is because XUV bursts generated in consecutive half-cycles of the field in (b) will have similar divergence properties because of the smooth radial structure of the beam.

The harmonic spectrum proves to also be a poor indicator of the XUV time structures. In Fig. 5(d) we show the cutoff region of the harmonic spectra generated by the two different laser pulses, after spatial filtering in the far field. Even though they correspond to very different time profiles, the two spectra are both strongly modulated and have similar shapes and cutoff energies. The modulation of the spectrum corresponding to the single attosecond burst is due to the presence of multiple, very weak satellite pulses in the time profile. We note that including a wider range of XUV energies into this time profile merely results in a shorter attosecond burst but does not otherwise alter the time structure.

The carrier envelope phase (CEP) of both laser pulses shown in Fig. 5 is zero with respect to a cosine oscillation. For the pulse shown in Fig. 5(b) there are no CEP values that lead to the selection of a single attosecond burst, and most CEP values in fact lead to more pronounced multiple peak pulses than the one shown in Fig. 5(c). In [14] we explored the CEP dependence of the far field selection of single attosecond pulses generated by a laser pulse with parameters as in Fig. 5(a), and showed that for most values of the CEP it is possible to isolate a single XUV burst. A laser pulse which has the same energy and is even more tightly focused than that in Fig. 5(a) (initial peak intensity of $12.6 \times 10^{14} \text{ W/cm}^2$ and a confocal parameter of 3 cm, as shown in Fig. 4) will also be strongly reshaped due to the ionization driven dynamics. Such a pulse also generates XUV radiation from which a single attosecond burst can be isolated for a range of CEP values.

These results allow us to conclude that in the absence of ionization driven spatiotemporal reshaping, it is not possible to generate isolated attosecond bursts by driving pulses with durations of three or more optical cycles. They also suggest that a large dynamical blueshift of such laser pulses can be used as a signature of the regime in which it is possible to isolate single attosecond bursts, since both the blueshift and the ability to select single attosecond pulses in the far field originate in the spatiotemporal reshaping driven by strong ionization dynamics.

IV. SUMMARY

In summary, we have analyzed the propagation and harmonic generation dynamics of an intense few-cycle laser pulse. We showed that the frequency modulation induced by rapid ionization in the nonlinear medium can be very large, and can indeed reach a value of 35% in conditions very similar to those in [1]. We demonstrated that whereas the

laser frequency modulation and the time structure of the generated XUV radiation is very sensitive to the initial focusing conditions, the harmonic spectrum is much less so. Our results indicate that a large frequency modulation and strong defocusing of the driving laser pulse after interaction with the nonlinear medium are signatures of the conditions that facilitate the selection of single attosecond bursts. However, our results also emphasize that a full characterization of the XUV time profile is possible only via direct temporal measurements, or alternatively via measurements of both the spectral strength and phase of the radiation.

ACKNOWLEDGMENTS

The authors are grateful to F. Krausz for discussions of the experiment in [1]. This material is based upon work supported by the Louisiana Board of Regents through Grant No. LEQSF(2004-07)-RD-A-09 and by the National Science Foundation through Grant No. PHY-0449235. R.K. acknowledges support from the Austrian Academy of Sciences.

-
- [1] M. Hentschel, R. Kienberger, Ch. Spielmann, G. A. Reider, N. Milosevic, T. Brabec, P. Corkum, U. Heinzmann, M. Drescher, and F. Krausz, *Nature (London)* **414**, 509 (2001).
- [2] S. C. Rae and K. Burnett, *Phys. Rev. A* **46**, 1084 (1992).
- [3] J. L. Krause, K. J. Schafer, and K. C. Kulander, *Phys. Rev. Lett.* **68**, 3535 (1992).
- [4] T. Brabec and F. Krausz, *Rev. Mod. Phys.* **72**, 545 (2000).
- [5] E. Priori, G. Cerullo, M. Nisoli, S. Stagira, S. De Silvestri, P. Villoresi, L. Poletto, P. Ceccherini, C. Altucci, R. Bruzzese, and C. de Lisio, *Phys. Rev. A* **61**, 063801 (2000).
- [6] Although the total electric field of course contains both the laser frequency and all the harmonic frequencies, we choose for technical reasons to propagate the electric fields for the laser radiation and the generated radiation separately: Since we are using a strong field description of the atomic response, the inclusion of the generated radiation in the driving field would give an incorrectly strong nonlinear atomic response to the higher frequencies.
- [7] B. L. Henke, E. M. Gullikson, and J. C. Davis, *At. Data Nucl. Data Tables* **54**, 181 (1993).
- [8] K. J. Schafer and K. C. Kulander, *Phys. Rev. Lett.* **78**, 638 (1997).
- [9] M. V. Ammosov, N. B. Delone, and V. P. Krainov, *Zh. Eksp. Teor. Fiz.* **91**, 2008 (1986) [*Sov. Phys. JETP* **64**, 1191 (1986)].
- [10] M. Lewenstein, Ph. Balcou, M. Yu. Ivanov, A. L'Huillier, and P. B. Corkum, *Phys. Rev. A* **49**, 2117 (1994).
- [11] The farfield mirror actually blocks a few mm of the central part of the laser beam. The calculated frequency modulation of the near-axis part of the laser beam after reflection on such a mirror is almost indistinguishable from the on-axis behavior as shown in Fig. 2(b).
- [12] A decrease of the cutoff energy as a result of defocusing has been studied in detail previously; see, for instance, K. Miyazaki and H. Takada, *Phys. Rev. A* **52**, 3007 (1995).
- [13] A. de Bohan, P. Antoine, D. B. Milosevic, and B. Piraux, *Phys. Rev. Lett.* **81**, 1837 (1998).
- [14] M. B. Gaarde and K. J. Schafer, *Opt. Lett.* **31**, 3188 (2006).